

# SOLVING THE MILD-SLOPE AND HELMHOLTZ EQUATIONS USING THE VIRTUAL ELEMENT METHOD (VEM), DEALING WITH HIGH ORDER ROBIN BOUNDARY CONDITION

R. Dupont<sup>1,2</sup> and M. Dauphin<sup>3</sup>, R. Mottier<sup>4,5,6</sup>

July 25, 2024

<sup>1</sup> GEOSCIENCES-M, Univ Montpellier, CNRS, Montpellier, France.

<sup>2</sup> IMAG, Univ Montpellier, CNRS, Montpellier, France.

<sup>3</sup> Scuola Superiore Meridionale, Napoli, Italy.

<sup>4</sup> École nationale des ponts et chaussées, France.

<sup>5</sup> Commissariat à l'énergie atomique et aux énergies alternatives, France.

<sup>6</sup> Institut national de recherche en sciences et technologies du numérique, France.

\*Corresponding authors. E-mail(s): [ronan.dupont@umontpellier.fr](mailto:ronan.dupont@umontpellier.fr);  
[mathias.dauphin-ssm@unina.it](mailto:mathias.dauphin-ssm@unina.it); [romain.mottier@outlook.com](mailto:romain.mottier@outlook.com).

## Abstract

The numerical solution of the Mild-slope equation (MSE) is crucial in various fields, including coastal engineering, oceanography, and offshore structure design. In this article, we present a novel approach utilizing the Virtual Element Method (VEM) for the numerical solution of the MSE. The VEM offers significant advantages over traditional finite element methods, particularly in handling complex geometries and irregular meshes. We first look at the implementation and validation of the model in the presence of Robin boundary conditions. We then apply the results to the calculation of eigenmodes for the port of Cherbourg.

**Keywords.** Mild-slope equation, Helmholtz equation, Virtual Element Method, computational fluid dynamics, validation, Finite Element Methods, Numerical Analysis, Complex Geometries, Irregular Meshes, Robin Boundary Condition, Coastal Engineering.

# 1 Introduction

Nowadays, coastal modeling has become a major challenge in the face of climate change. Coastal-related topics have become very numerous, including ocean modeling (large-scale), port modeling and numerous other topics such as morphodynamics. In this study, we are particularly interested in port modeling through the equation models developed by Helmholtz (1868) and Berkhoff (1972). These two equation models can be used in coastal modeling to calculate wave agitation inside a harbor. The Helmholtz (1868) equation is a very classical equation, which can be used in various fields such as electromagnetics or acoustics. In our study, it is used for flat sea bottoms, while the Berkhoff (1972) equation, also known as the Mild-Slope equation, is used for variable bottoms with a maximum slope of 1/3 (Booij 1983). In this study, we have chosen to solve these equations using the virtual element method (Beirão da Veiga et al. 2014) MATHIAS, tu peux ajouter qqsls autres refs importantes stp (refs.bib). This method has the advantage of i) being a high-order finite element method, which enables wave phenomena to be accurately captured, where simple finite elements have difficulty capturing them RORO, tu peux ajouter des références pour ce que tu disais, que sur des méthodes FEM simple, même en raffinant, on arrivait pas à capturer tous les phénomènes ondulatoires, ii) handle polyhedral meshes as well as non-conforming meshes, enabling simple refinement in certain areas. Although a few studies have already dealt with the Helmholtz (1868) problem in virtual elements (Perugia et al. 2016; Mascotto et al. 2019), none of them has had any concrete application in the coastal sector. In this study, we will first express the modeling of the problem. Next, we will explain the virtual element strategy for approximating this problem. Finally, we'll look at a particular boundary condition, the Robin condition. After validating our model, we will apply it to the calculation of eigenvalues for the port of Cherbourg.

(Cook et al. 2021)

Vous pouvez étoffer un peu, c'est un draft.

## 2 Model Problem

In this section, we consider the wave problem described in figure 1.

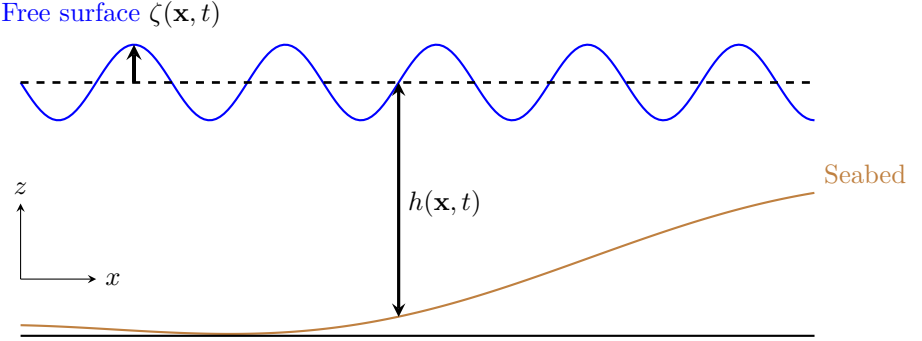


**Figure 1:** Sketch of a free surface elevation  $\zeta$  in the  $(x, z)$ -plane.

with  $\zeta$  the free surface defined by  $\zeta(\mathbf{x}, t) = \Re\{\eta(x, y) e^{-i\omega t}\}$ ,  $\eta$  a complex-valued amplitude of  $\zeta$ ,  $\omega = 2\pi/T_0$  the angular frequency,  $T_0$  the wave period and  $h$  the depth.

The amplitude  $\eta$  can be split into its incident and reflective part,

$$\eta = \eta_I + \eta_R.$$

We thus have,

$$\eta_I(\mathbf{x}, t) = a_I(\mathbf{x})e^{-i\omega t} \quad \text{and} \quad \eta_R(\mathbf{x}, t) = a_R(\mathbf{x})e^{-i\omega t}$$

with the incident wave amplitude defined by,

$$a_I(\mathbf{x}) = a_{\max} e^{-i\mathbf{k}\mathbf{x}} \quad \text{with} \quad \mathbf{k} = k(\cos(\theta), \sin(\theta))^T,$$

with  $\theta$  the incident wave angle,  $a_{\max}$  the maximum wave amplitude.

The amplitude of the reflected wave  $a_R$  is obtained by solving the Helmholtz (1868) equation, in the case of a flat bottom,

$$\begin{cases} \Delta a + k^2 a = 0, & \text{in } \Omega, \\ a = a_I, & \text{in } \Gamma_{\text{in}}, \\ \frac{\partial a}{\partial n} + ik a = 0, & \text{in } \Gamma_{\text{out}}, \\ a = -\gamma a_I & \text{in } \Gamma_D. \end{cases} \quad (1)$$

with  $\gamma \in [0, 1]$  the reflection coefficient,  $k$  the wave number: solution of the dispersion relation at order 1 (equation (2)) from linear theory (Airy 1845),

$$\omega^2 = g k \tanh(kh) \quad \text{with} \quad \omega = \frac{2\pi}{T_0}. \quad (2)$$

The amplitude of the reflected wave  $a_R$  can also be obtained by solving the Mild-Slope equation (Berkhoff 1972), in the case of a variable bottom,

$$\left\{ \begin{array}{ll} \nabla(C_p C_g \nabla a) + k^2 C_p C_g a = 0, & \text{in } \Omega, \\ a = a_I, & \text{in } \Gamma_{\text{in}}, \\ \frac{\partial a}{\partial n} + ik a = 0, & \text{in } \Gamma_{\text{out}}, \\ a = -\gamma a_I & \text{in } \Gamma_{\text{D}}. \end{array} \right. \quad (3)$$

with

$$C_p = \frac{\omega}{k} \quad \text{and} \quad C_g = \frac{1}{2} C_p \left[ 1 + kh \frac{1 - \tanh^2(kh)}{\tanh(kh)} \right]. \quad (4)$$

The choice of boundary conditions will be explained in the application section 4.

### Remarks:

- In practice,  $k$  is obtained simply by using the Guo (2002) approximation.
- Assuming constant depth within the port and  $C_g = C_p/2$  (as in shallow water) and noting that  $C_p = \omega/k = Cte$ , equation (3) can be simplified to yield the Helmholtz (1868) equation.

## 3 Solving Equations Using the Virtual Element Method

In this section, we develop the variational formulation of the problem and briefly recall the formalism of virtual elements to solve the problem.

Eventuellement à completer.

### 3.1 Basic Settings of Virtual Element Method

Introduire un peu de VEM

### 3.2 Variational formulation

We decompose this subsection into two parts, one expressing the variational formulation for the Helmholtz (1868) equation (1) and another for that of the Mild-Slope equation (3).

#### 3.2.1 The Helmholtz Equation

We consider the Helmholtz (1868) equation (1) and thus the following variational formulation:

$$\begin{cases} \text{find } u \in V = H_0^1(\Omega) \text{ such that} \\ \quad \mathcal{A}(u, v) = 0 \quad \forall v \in V, \end{cases} \quad (5)$$

where,

$$\begin{aligned} \mathcal{A}(u, v) &= \int_{\Omega} \Delta u v + k^2 \int_{\Omega} u v, \\ &\stackrel{\text{green}}{=} - \int_{\Omega} \nabla u \nabla v + k^2 \int_{\Omega} u v + \int_{\Gamma_{\text{out}}} \frac{\partial u}{\partial n} v, \\ &\stackrel{\partial u / \partial n = -iku}{=} - \underbrace{\int_{\Omega} \nabla u \nabla v + k^2 \int_{\Omega} u v}_{a} - i \underbrace{\int_{\Gamma_{\text{out}}} k u v}_{r}, \\ &= a(u, v) + r(u, v). \end{aligned} \quad (6)$$

with  $r(u, v) = -i \int_{\Gamma_{\text{out}}} k u v$  the bilinear form due to the Robin boundary condition.

We build a discrete problem in following form:

$$\begin{cases} \text{find } u_h \in V_h \subset V \text{ such that} \\ \quad \mathcal{A}_h(u_h, v_h) = 0 \quad \forall v_h \in V_h, \end{cases} \quad (7)$$

where  $V_h \subset V$  is a finite dimensional space and  $\mathcal{A}_h(\cdot, \cdot) : V_h \times V_h \rightarrow \mathbb{R}$  is a discrete bilinear form approximating the continuous form  $\mathcal{A}(\cdot, \cdot)$ .

We thus have the discrete form:

$$\begin{aligned} \mathcal{A}_h(u_h, v_h) &\stackrel{\text{green}}{=} \sum_{E \in \Omega_h} \left[ - \int_E \nabla u_h \nabla v_h + \int_E u_h v_h - \mathbb{1}_{\Gamma_{\text{out}} \subset E} i \int_{\Gamma_{\text{out}}} k u_h v_h \right], \\ &= a_h(u_h, v_h) + r_h(u_h, v_h). \end{aligned} \quad (8)$$

with  $a_h$  and  $r_h$  the discrete forms of  $a$  and  $r$ ,  $\mathbb{1}_{\Gamma_{\text{out}} \subset E}$  the indicator function and  $u = u + u_D$  and  $u_D$  is the lifting of  $-\gamma a_I$  or  $a_I$  (depending on the border).

### 3.2.2 The Mild-Slope Equation

Now, we consider the Berkhoff (1972) equation (3) and thus the following variational formulation:

$$\begin{cases} \text{find } u \in V = H_0^1(\Omega) \text{ such that} \\ \quad \mathcal{A}(u, v) = 0 \quad \forall v \in V, \end{cases} \quad (9)$$

where,

$$\mathcal{A}(u, v) = \int_{\Omega} \nabla(C_p C_g \nabla u) v + \int_{\Omega} k^2 C_p C_g u v . \quad (10)$$

We build a discrete problem in following form:

$$\begin{cases} \text{find } u_h \in V_h \subset V \text{ such that} \\ \mathcal{A}_h(u_h, v_h) = 0 \quad \forall v_h \in V_h, \end{cases} \quad (11)$$

where  $V_h \subset V$  is a finite dimensional space and  $\mathcal{A}_h(\cdot, \cdot) : V_h \times V_h \rightarrow \mathbb{R}$  is a discrete bilinear form approximating the continuous form  $\mathcal{A}(\cdot, \cdot)$ .

We thus have the discrete form:

$$\begin{aligned} \mathcal{A}_h(u_h, v_h) &= \sum_{E \in \Omega_h} \left[ \int_E \nabla(C_p C_g \nabla u_h) v_h + \int_E k^2 C_p C_g u_h v_h \right], \\ &\stackrel{1/E \int_E C_p C_g = \mathcal{A}_E}{\approx} \sum_{E \in \Omega_h} \left[ \mathcal{A}_E \int_E (\Delta u_h) v_h + \mathcal{B}_E \int_E u_h v_h \right], \\ &\stackrel{\substack{1/E \int_E k^2 C_p C_g = \mathcal{B}_E \\ \partial u / \partial n = -iku}}{=} \sum_{E \in \Omega_h} \left[ -\mathcal{A}_E \int_E \nabla u_h \nabla v_h + \mathcal{B}_E \int_E u_h v_h - \mathbb{1}_{\Gamma_{\text{out}} \subset E} i \mathcal{A}_E \int_{\Gamma_{\text{out}}} k u_h v_h \right], \\ &= a_h(u_h, v_h) + r_h(u_h, v_h) . \end{aligned} \quad (12)$$

with  $a_h$  and  $r_h$  the discrete forms of  $a$  and  $r$ : defined in the same way as above,  $\mathbb{1}_{\Gamma_{\text{out}} \subset E}$  the indicator function and  $u = u + u_D$  and  $u_D$  is the lifting of  $-\gamma a_I$  or  $a_I$  (depending on the border).

**Remark:** Unlike the discrete formulation of the homogeneous [Helmholtz \(1868\)](#) equation (8), the discrete formulation of the Mild-Slope equation (12) assumes that  $k^2$  and  $C_p C_g$  are constant for each cell in the mesh.

### 3.3 Robin Boundary Condition

In this section, we focus on calculating Robin's term  $r_h(u_h, v_h)$  in our variational formulation. Unlike the mass matrix  $M$  and the stiffness matrix  $K$ , which are calculated using the virtual element formalism, the robin matrix  $R$  is calculated in a manner analogous to conventional high-order finite elements, with the difference that the degrees of freedom are not placed in the same locations.

We can express the global matrix  $R$  associated to the formulation  $r_h$  in a basis of classical shape function, with thus  $R = \left( \int_{\Gamma_{\text{out}}} \alpha(x, y) \Phi_j(x, y), \Phi_i(x, y) \right)_{i,j}$  with  $\alpha$  any function of  $\mathbb{R}^2$ .

The  $\Gamma_{\text{out}}$  boundary can be decomposed into a sum of 1D elements that can be characterized by the segment  $[\xi_0, \xi_0 + \lambda]$  between two points  $V_0$  and  $V_1$ . These elements are segments joining 2 consecutive points of the edge. The  $\Phi_i$  basis function attached to the  $i$  vertex of the edge, restricted to the edge element, is a  $\mathbb{P}_k$  function of the edge. These characteristic 1D elements are shown in the figure 2 with the degrees of freedom corresponding to the Gauss-Lobatto quadrature points on  $[0, \lambda]$ . Consequently, the higher the order, the more points there will be on the segment.

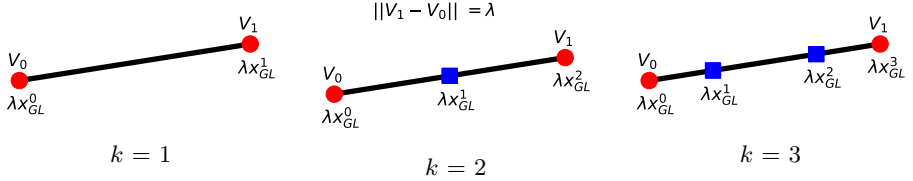


**Figure 2:** 1D element  $[\xi_0, \xi_0 + \lambda]$  representation for different orders  $k$ , with ● : Summits dofs, ■ : Edges dofs.

In this way, we can express the segment's local matrix:

$$R_{\text{local}} = \left( \int_0^\lambda \alpha_*(\xi_0 + \xi) \varphi_j(\xi) \varphi_i(\xi) d\xi \right)_{0 \leq i, j \leq k} \quad (13)$$

with  $\varphi_i, \varphi_j$  polynomials of order  $k$ ,  $\alpha_*(\xi_0 + \xi) = \alpha(V_0 + \xi \vec{t})$  the 1D restriction of  $\alpha$  on  $\Gamma_{\text{out}}$  and  $\vec{t}$  the tangential unit vector (from  $V_0$  to  $V_1$ ).

We can easily deduce the explicit form of  $\varphi_{i=0, \dots, k}$  because we have  $\forall i, j \in \llbracket 0, k \rrbracket$ ,

$$\varphi_i(\lambda x_{GL}^j) = \delta_j^i, \quad (14)$$

with  $x_{GL}^j$  the  $j - th$  Gauss-Lobatto quadrature point on  $[0, 1]$  (see figure 2). We can therefore deduce from the Lagrange polynomials:

$$\begin{aligned} \varphi_i(\xi) &= \sum_{j=0}^k \delta_j^i \left( \prod_{l=0, l \neq j}^k \frac{\xi - \lambda x_{GL}^l}{\lambda x_{GL}^j - \lambda x_{GL}^l} \right), \\ &= \frac{1}{\lambda^k} \prod_{l=0, l \neq i}^k \frac{\xi - \lambda x_{GL}^l}{x_{GL}^i - x_{GL}^l}. \end{aligned}$$

Conclure avec le calcul de l'intégrale, corriger l'algorithme avec les notations, réduire/traduire remarque

---

**Algorithm 1** Pseudocode with Robin Boundary Conditions

---

```

1: for  $E \in \mathcal{T}_h$  do
2:    $\mathcal{A}_h \leftarrow \mathcal{A}_h + \mathcal{A}_h^E$ 
3:    $l_h \leftarrow l_h + l_h^E$ 
4: end for
5: for  $e \in \mathcal{E}_h^b$  do
6:   if  $e \in \mathcal{E}_h^{b,r}$  then
7:      $\mathcal{A}_h \leftarrow \mathcal{A}_h + \textcolor{red}{R}_h^e$ 
8:      $l_h \leftarrow l_h + l_h^e$ 
9:   else if  $e \in \mathcal{E}_h^{b,d}$  then
10:     $\mathcal{A}_h^e \leftarrow 1$ 
11:     $l_h^e \leftarrow \text{value of DBC}$ 
12:   end if
13: end for

```

---

**Remark:**

$$\begin{aligned}
& \left( \int_0^\lambda \alpha_*(\xi_0 + \xi) \varphi_j(\xi) \varphi_i(\xi) d\xi \right)_{0 \leq i,j \leq k} \\
&=_{\alpha_*=\alpha=cte} \left( \frac{\alpha}{\lambda^{2k}} \int_0^\lambda \left[ \prod_{l=0, l \neq i}^k \frac{\xi - \lambda x_{\text{GL}}^l}{x_{\text{GL}}^i - x_{\text{GL}}^l} \prod_{l=0, l \neq i}^k \frac{\xi - \lambda x_{\text{GL}}^l}{x_{\text{GL}}^j - x_{\text{GL}}^l} \right] d\xi \right)_{0 \leq i,j \leq k} \\
&=_{\substack{\xi=\lambda\xi' \\ d\xi=\lambda d\xi'}} \left( \frac{\alpha}{\lambda^{2k}} \int_0^1 \left[ \prod_{l=0, l \neq i}^k \frac{\lambda \xi' - \lambda x_{\text{GL}}^l}{x_{\text{GL}}^i - x_{\text{GL}}^l} \prod_{l=0, l \neq i}^k \frac{\lambda \xi' - \lambda x_{\text{GL}}^l}{x_{\text{GL}}^j - x_{\text{GL}}^l} \right] \lambda d\xi' \right)_{0 \leq i,j \leq k} \\
&= \left( \frac{\alpha}{\lambda^{2k}} \int_0^1 \left[ \prod_{l=0, l \neq i}^k \lambda \frac{\xi' - x_{\text{GL}}^l}{x_{\text{GL}}^i - x_{\text{GL}}^l} \prod_{l=0, l \neq i}^k \lambda \frac{\xi' - x_{\text{GL}}^l}{x_{\text{GL}}^j - x_{\text{GL}}^l} \right] \lambda d\xi' \right)_{0 \leq i,j \leq k} \\
&= \left( \alpha \lambda \int_0^1 \left[ \prod_{l=0, l \neq i}^k \frac{\xi' - x_{\text{GL}}^l}{x_{\text{GL}}^i - x_{\text{GL}}^l} \prod_{l=0, l \neq i}^k \frac{\xi' - x_{\text{GL}}^l}{x_{\text{GL}}^j - x_{\text{GL}}^l} \right] d\xi' \right)_{0 \leq i,j \leq k} \\
&= \alpha \lambda \left( \int_0^1 \tilde{\varphi}_j(\xi) \tilde{\varphi}_i(\xi) d\xi \right)_{0 \leq i,j \leq k}
\end{aligned} \tag{15}$$

with  $\tilde{\varphi}_i$  the polynomials for a unit element  $[\xi_0, \xi_0 + 1]$

Et par exemple pour  $k = 1$ ,  $\varphi_1(\xi) = \frac{\lambda - \xi}{\lambda}$ ,  $\varphi_2(\xi) = \frac{\xi}{\lambda}$ .

Pour le cas particulier où  $\alpha = cte$ , l'intégrale (13) revient à intégrer un polynôme de degrés  $2k$ . En évaluant celle-ci par  $k + 2$  points de GL (car exacte à  $2n - 3$ ), on obtient l'intégrale exacte.

Nous allons construire également le second membre  $SMB$  qui provient des

termes de bord inhomogènes:

$$SMB_i = \int_{\partial\Omega} b(x, y)\Phi_i(x, y).$$

Ce terme est non trivialement nul si le sommet  $i$  appartient à  $\partial\Omega = \Gamma_b \cup \Gamma_t \cup \Gamma_l \cup \Gamma_r$ . Pour un élément de référence de la forme  $[\xi_0, \xi_0 + \delta]$ , le vecteur élémentaire associé à ce terme inhomogène est de la forme

$$vecb = \left( \int_0^\lambda b_*(\xi_0 + \xi)\varphi_i(\xi) d\xi \right)_{1 \leq i \leq k+1},$$

avec  $\varphi_1(\xi) = \frac{\delta - \xi}{\delta}$ ,  $\varphi_2(\xi) = \frac{\xi}{\delta}$  et  $\beta_*(\xi_0 + \xi)$  coïncide avec  $\beta_*(\xi_0 + \xi) = \beta(V_0|_x + \xi t_x, V_0|_y + \xi t_y)$  et  $\vec{t}$  est le vecteur unitaire orienté de  $V_0$  à  $V_1$ . Également, cette intégrale pourra être intégrée par GL.

### 3.4 Numerical Validation

In this section, we check the validity of our model. Thus, we compare our model with a manufactured analytical solution (see appendix A). We therefore consider the Helmholtz (1868) equation with mixed Dirichlet and Robin boundary conditions, below equation (16).

$$\begin{cases} \Delta u + k^2 u = f(x, y) & , \quad \text{in } \Omega, \\ u = u_{\text{exact}} & , \quad \text{on } \Gamma_2 \cup \Gamma_3 \cup \Gamma_4, \\ \frac{\partial u}{\partial n} + i k u = g(x, y) & , \quad \text{on } \Gamma_1, \end{cases} \quad \begin{array}{c} \Gamma_3 \\ \square \\ \Gamma_4 \quad \Omega \quad \Gamma_2 \\ \Gamma_1 \end{array} \quad (16)$$

For this analytical case, we take the geometry of a unit square and link it with regular triangles, irregular triangles, irregular quadrilaterals and polygons. To generate these meshes, we use the Gmsh (Geuzaine et al. 2009) and PyPoly-Mesher (Abedi-Shahri 2024; Talisch et al. 2012). We perform calculations from order 1 to order 5 on maximum cell diameters  $h$  from 0.05 to 0.7 m. We then compute the  $L^2$  error for each calculation. The results are shown in figure 3.

We find the expected superconvergence of order  $\mathcal{O}(h^{k+1})$ .

**Remarks:** For a validation with the Mild-Slope equation, the order would have been less good, given the approximation we have made per cell.

## 4 Application and Discussion

In this section, we apply the solution of the Helmholtz and Mild-Slope equations to a coastal engineering problem. We take the case of the port of Cherbourg in France and calculate the associated wave fields under certain conditions. First, we select our study site, as shown in figure 4 (left). Next, we

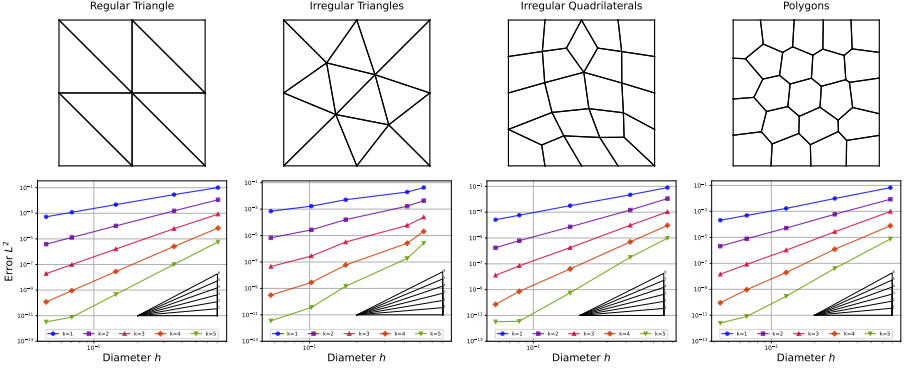


**Figure 3:** Convergence of order  $\mathcal{O}(h^{k+1})$ .

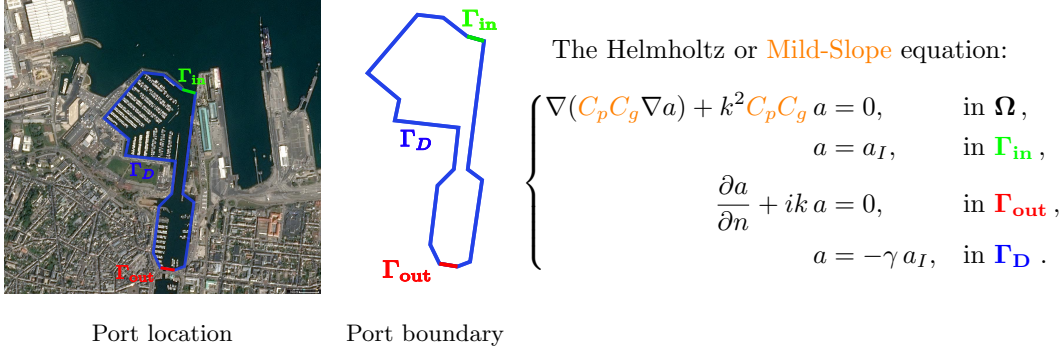


**Figure 4:** Configuration of our study of the port of Cherbourg

break down the contour into 3 different boundaries (figure 4 (center)):  $\Gamma_{\text{in}}$  the harbour entrance,  $\Gamma_{\text{out}}$  the harbour exit and  $\Gamma_{\text{D}}$  the port walls. Finally, we assign the correct boundary condition to these edges (figure 4 (right)).

The  $\Gamma_{\text{in}}$  boundary condition is modeled by an inhomogeneous Dirichlet condition taking the incident field as argument. The  $\Gamma_{\text{out}}$  boundary condition is modeled by a Robin condition allowing the wave to exit without disturbing other wave fields. More information on this condition in Appendix B. The  $\Gamma_{\text{D}}$  boundary condition is modeled by an inhomogeneous Dirichlet condition with a reflection coefficient  $\gamma$ . First, we'll look at the importance of this reflection coefficient in the section 4.1. Then, we will compare the results obtained using the Helmholtz equation and the Mild-Slope equation, in section 4.2. Finally, we will compare the results with different orders of the virtual element method, in section 4.3.

## 4.1 Sensitivity of the $\gamma$ reflection coefficient

In this section, we look at the influence of the harbor wall reflection coefficient  $\gamma$  on wave fields. We compare reflected and total wave fields for two different reflection coefficients,  $\gamma = 1$  (figure 5 (top)) and  $\gamma = 0.5$  (figure 5 (bottom)). For this study, we generate an incident wave field entering the harbour at  $280^\circ$  with a maximum amplitude  $a_{\max} = 1$  m and a wave period  $T_0 = 8$  s. This incident field can be seen in figure 5 (left). The results of this study are shown in figure 5 with i) on the left, the incident field ii) in the middle, the reflected field (solution of the Helmholtz equation) iii) on the right, the total field.

### Solving the Helmholtz problem with $\gamma = 1$

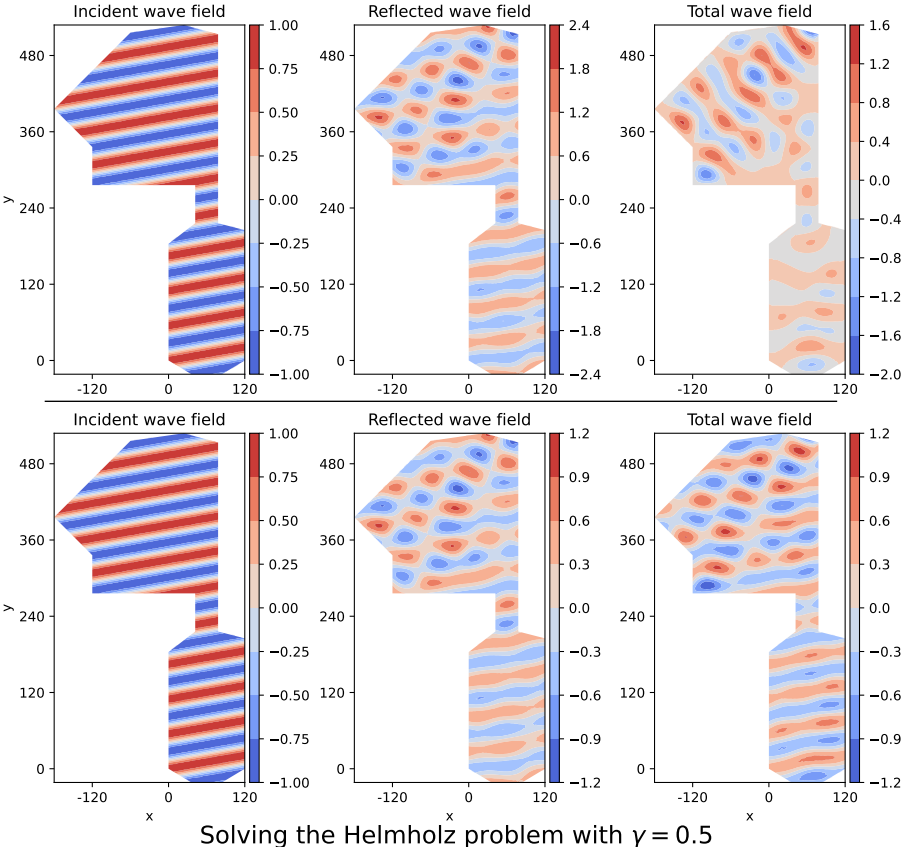


**Figure 5:** Comparison of wave fields for the two reflection coefficients  $\gamma = 1$  (top) and  $\gamma = 0.5$  (bottom). Problem condition:  $\alpha = 280^\circ$ ,  $a_{\max} = 1$  m and  $T_0 = 8$  s.

The results in figure 5 show that by halving the reflection coefficient  $\gamma$ , the reflected wave field is also halved. This results in a totally different total wave field (incident + reflected), so that the harbour's eigenmodes are no longer located in exactly the same places for the two configurations. It is therefore very important to calibrate this reflection condition correctly.

Ajouter note sur le fait que tous les murs renvoient la même condition de bord alors que c'est peut-être pas vrai partout ?

## 4.2 Bottom sensitivity between Helmholtz and Mild-Slope

In this section, we look at the influence of the sea bottom on wave fields. We compare a simulation with a flat bottom at a depth of 5 m (figure 6 top left) using the Helmholtz model, with a linear bottom (figure 6 bottom left) using the Mild-Slope model. For this study, we generate an incident wave field

entering the harbour at  $280^\circ$  with a maximum amplitude  $a_{\max} = 2$  m and a wave period  $T_0 = 8$  s. To make the modelling more realistic, Munk (1949) breaking wave criterion is added. This decreases wave amplitude linearly with depth. This incident field can be seen in figure 6. The results of this study are shown in figure 6 from left to right: i) the depth ii) the incident field iii) the reflected field iv) the total field.

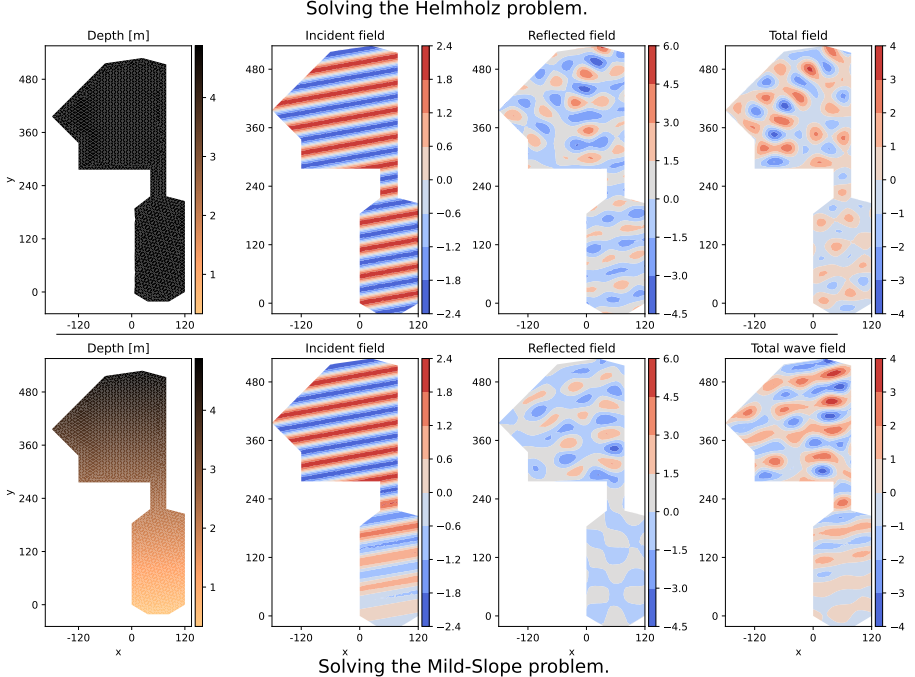


**Figure 6:** Comparison of wave fields for two different sea bottom: a flat bottom (top) and a linear bottom (bottom). Problem condition:  $\alpha = 280^\circ$ ,  $a_{\max} = 2$  m and  $T_0 = 8$  s.

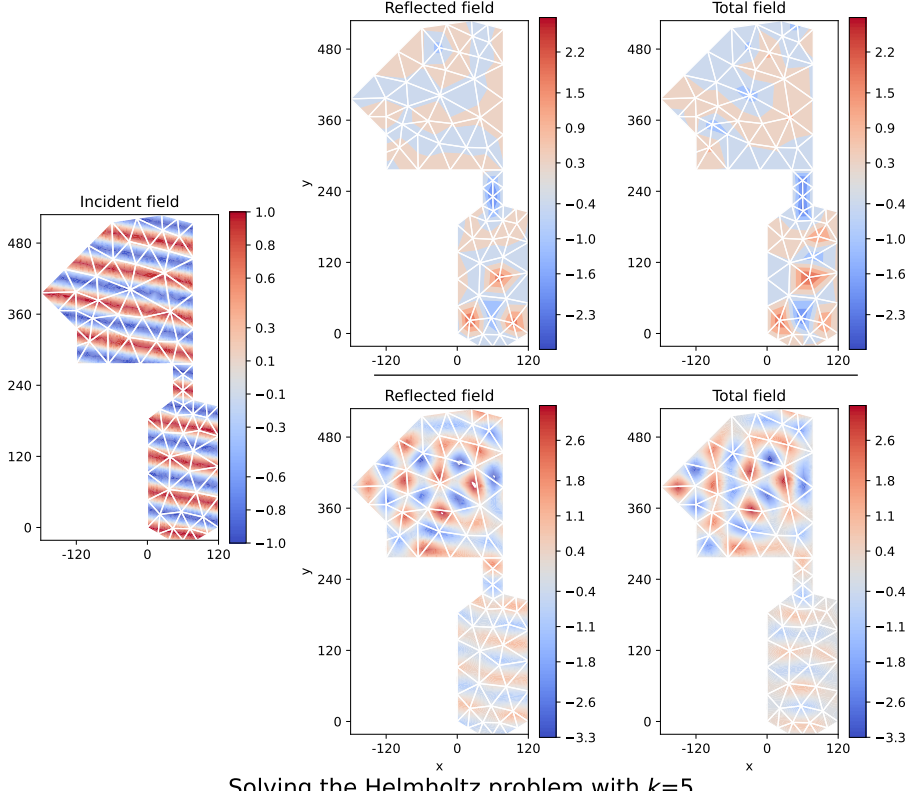
The results in figure 6 show that the lack of depth limits the formation of eigenmodes. In fact, in the flat-bottom simulation (top), eigenmodes are formed in the upper and lower parts of the harbor; whereas in the linear-bottom simulation (bottom), eigenmodes are no longer formed where there is almost no water: in the lower part of the harbor.

### 4.3 Sensitivity to order of resolution

In this section, we look at the influence of the order of solution of the virtual element method on the solution of the Helmholtz problem. We compare the reflected and total wave fields for two orders of resolution with fairly coarse mesh (figure 7), order 1 (figure 7 top) with 81 degrees of freedom and order 5 (figure 7 bottom) with 881 degrees of freedom. For this study, we generate an

incident wave field entering the harbour at  $250^\circ$  with a maximum amplitude  $a_{\max} = 1$  m and a wave period  $T_0 = 8$  s. The results of this study are shown in figure 7 with i) on the left, the incident field ii) in the middle, the reflected field (solution of the Helmholtz equation) iii) on the right, the total field.

### Solving the Helmholtz problem with $k=1$



### Solving the Helmholtz problem with $k=5$

**Figure 7:** Comparison of wave fields for the two order of resolution  $k = 1$  (top) and  $k = 5$  (bottom). Problem condition:  $\alpha = 250^\circ$ ,  $a_{\max} = 1$  m and  $T_0 = 8$  s.

The results in figure 7 show the importance of a high-order solution method for this kind of problem. Indeed, we note that with order 1, it's very difficult to capture the port's eigenmodes, whereas with order 5, the port's eigenmodes are distinguishable.

## 5 Conclusion

Blablabla

## 6 Declarations

### 6.1 Availability of data and material

All data, models, and code generated or used during the study are available on request.

### 6.2 Conflict of interest

The authors declare that they have no conflict of interest.

### 6.3 Acknowledgements

This work was conducted as part as M. Dupont's PhD studies which is funded by the CNRS with the MITI grant. We gratefully acknowledge funding from CNRS, OPTIBEACH projects and FEDER Europe. We would also like to thank Pr. Bouchette Frédéric for his ideas.

## Appendix

### A Manufactured analytical solution

The solution to the equation 16 problem has been produced using the following functions:

$$\begin{aligned} u_{\text{exact}}(x, y) &= (x + y) \cdot (1 + i) + \exp(x^2 + i y^2), \\ f(x, y) &= -((2x)^2 + (2i y)^2 + 2(1 + i)) \cdot \exp(x^2 + i y^2) + k^2 \cdot u_{\text{exact}}(x, y), \\ g(x, y) &= (1 + i) + (2i y) \cdot \exp(x^2 + i y^2) + i k \cdot u_{\text{exact}}(x, y). \end{aligned} \tag{A1}$$

This produces the complex analytical solution that can be seen below in figure A1.

### B Interest of a Robin condition

To show the interest of a Robin boundary condition in our problem, we look at the problem represented by figure B1. In this problem, we want to calculate the amplitude of reflected waves around an island. Thus, we have an incident wave arriving at  $0^\circ$  with an amplitude of 2 m and a period of 20 s. This wave is reflected on the boundary island  $\Gamma_D$ . On the other hand, the wave must be able to leave the domain freely via the boundary  $\Gamma_{\text{inf}}$ .

The reflected wave is calculated by the following Helmholtz (1868) equation and the wave leaving condition at infinity  $\Gamma_{\text{inf}}$  will be studied for a Robin (left) and zero Neumann (right) condition.

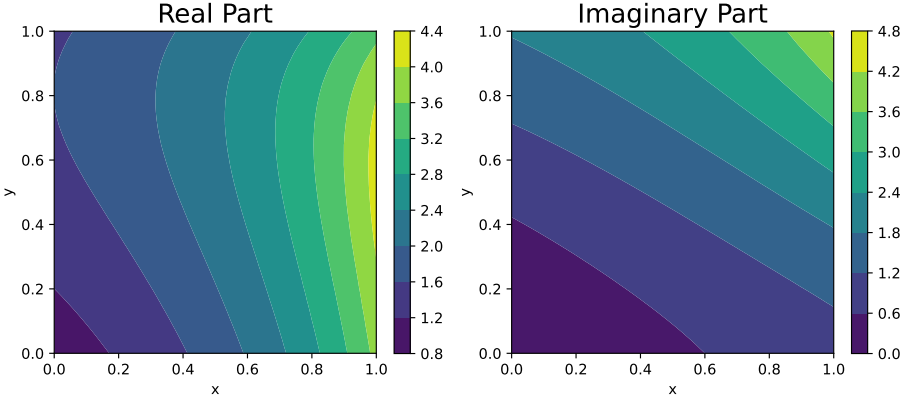


**Figure A1:** Real and Imaginary part of  $u_{\text{exact}}$ .

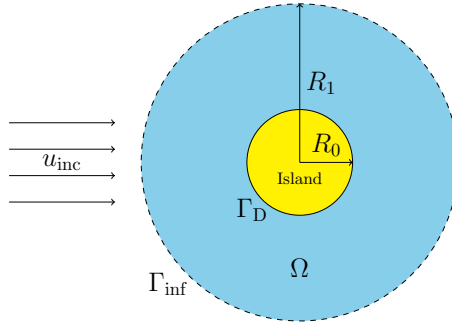


**Figure B1:** Sketch of the island reflection problem.

$$\left\{ \begin{array}{l} \Delta u + k^2 u = 0 \\ u = -u_{\text{inc}} \\ \frac{\partial u}{\partial n} + i k u = 0 \end{array} \right. , \quad \text{in } \Omega, \quad \text{or} \quad \left\{ \begin{array}{l} \Delta u + k^2 u = 0 \\ u = -u_{\text{inc}} \\ \frac{\partial u}{\partial n} = 0 \end{array} \right. , \quad \text{on } \Gamma_{\text{Inf}}.$$

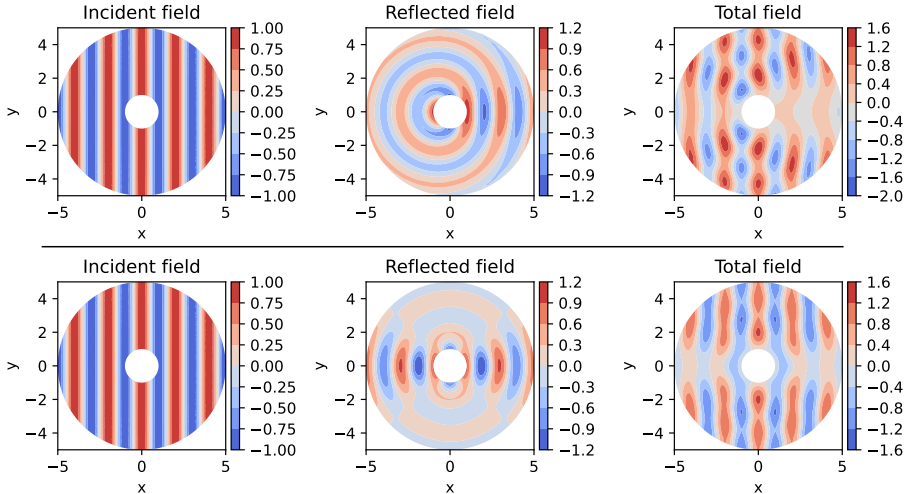
The results of this study are shown in figure B2. In this figure, it's clear that the wave reflected under Robin's condition (top) can leave freely, while the wave reflected under Neumann's condition (bottom) seems to be disturbed under this condition.

## C Notes

### C.1 Dofs

Let  $\Omega_h$  be a simple polygonal mesh on  $\Omega$ . This can be any decomposition of  $\Omega$  in non overlapping polygons  $E$  with straight faces. The space  $V_h$  will be

## Solving the Helmholtz problem with a Robin condition on $\Gamma_{\text{inf}}$



## Solving the Helmholtz problem with a Neuman condition on $\Gamma_{\text{inf}}$

**Figure B2:** Comparison of the results obtained on the island problem by solving the Helmholtz equation with a Robin condition (top) and a zero Neumann condition (bottom).

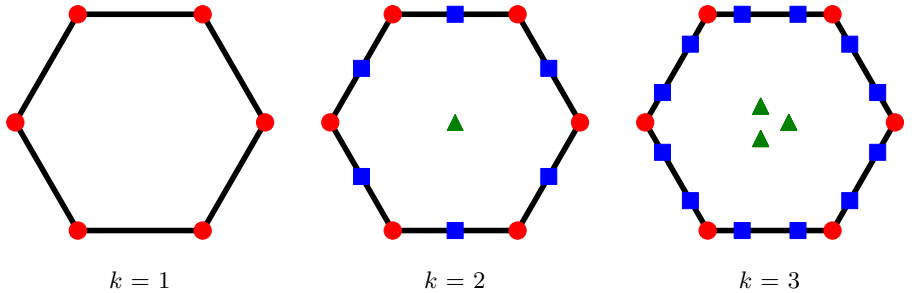


**Figure C3:** 2D element with ● : Summits dofs, ■ : Edges dofs, ▲ : Inner dofs.

defined element-wise, by introducing

- local spaces  $V_{h|E}$ ;
- the associated local degrees of freedom.

For all  $E \in \Omega_h$  :

$$V_{h|E} = \left\{ v_h \in H_0^1(\Omega) \cap C^0(\partial E) : v_h|_{\partial E} \in \mathbb{P}_k(E), \Delta v_h \in \mathbb{P}_k(E) \right. \\ \left. (\Pi_k^\nabla v_h - v_h, p)_{0,E} = 0, \forall p \in \mathbb{P}_k(E)/\mathbb{P}_{k-2}(E) \right\} \quad (\text{C1})$$

where  $\mathbb{P}_k(E)/P_{k-2}(E)$  is the subspace of  $\mathbb{P}_k(E)$  of the polynomials that are orthogonal in the sense of  $L^2$  to  $\mathbb{P}_{k-2}(E)$ , or, alternatively, the polynomials of degree  $k-1$  and  $k$ .

- the functions  $V_{h|E}$  are continuous (and known) on  $\partial E$ ;
- the functions  $V_{h|E}$  are unknown on  $E$ !

1. Mesh Decomposition: We consider a polytopal decomposition  $\{T_h\}_h$  of the domain  $\Omega$  which is regular—that is, there exists  $\rho \in (0, 1)$ , independent of  $h$ , such that every element  $E \in T_h$  is star-shaped with respect to a ball of radius  $\geq \rho h_E$ , with  $h_E$  the diameter of  $E$ .

2. Local Projections: We denote by  $\Pi_k^{\nabla, E} : H^1(E) \rightarrow \mathbb{P}_k(E)$  and  $\Pi_k^{0, E} : L^2(E) \rightarrow \mathbb{P}_k(E)$  the usual local elliptic projection and local  $L^2$ -projection respectively onto the space of polynomials of degree at most  $k$ .

3. Virtual Space: We define the local virtual space by

$$V_h^E = \left\{ v_h \in H_0^1(\Omega) \cap C^0(\partial E) : v_h|_{\partial E} \in \mathbb{P}_k(E), \Delta v_h \in \mathbb{P}_k(E) \right. \\ \left. (\Pi_k^{\nabla} v_h - v_h, p)_{0,E} = 0, \forall p \in \mathbb{P}_k(E)/\mathbb{P}_{k-2}(E) \right\}$$

where  $\mathbb{P}_k(E)/P_{k-2}(E)$  is the subspace of  $\mathbb{P}_k(E)$  of the polynomials that are orthogonal in the sense of  $L^2$  to  $\mathbb{P}_{k-2}(E)$ , or, alternatively, the polynomials of degree  $k-1$  and  $k$ .

3. DDL

4. Base:

$$m_{\alpha_1, \alpha_2} = \left( \frac{x - x_D}{h_D} \right)^{\alpha_1} \cdot \left( \frac{y - y_D}{h_D} \right)^{\alpha_2}$$

## References

- Abedi-Shahri, Seyed Sadjad (2024). *pyPolyMesher: Generation of Polygonal Mesh*. DOI: [10.5281/ZENODO.12794558](https://doi.org/10.5281/ZENODO.12794558).
- Airy, George Biddell (1845). *Tides and waves*. B. Fellowes.
- Beirão da Veiga, L., F. Brezzi, L. D. Marini, and A. Russo (2014). “The Hitch-hiker’s Guide to the Virtual Element Method”. In: *Mathematical Models and Methods in Applied Sciences* 24.08, pp. 1541–1573. DOI: [10.1142/S021820251440003X](https://doi.org/10.1142/S021820251440003X).
- Berkhoff, J.C.W. (1972). “COMPUTATION OF COMBINED REFRACTION - DIFFRACTION”. In: *Coastal Engineering Proceedings* 1.13, p. 23. DOI: [10.9753/icce.v13.23](https://doi.org/10.9753/icce.v13.23).
- Booij, N. (1983). “A note on the accuracy of the mild-slope equation”. In: *Coastal Engineering* 7.3, pp. 191–203. DOI: [https://doi.org/10.1016/0378-3839\(83\)90017-0](https://doi.org/10.1016/0378-3839(83)90017-0).
- Cook, Megan, Frédéric Bouchette, Bijan Mohammadi, Léa Sprunck, and Nicolas Fraysse (2021). “Optimal Port Design Minimizing Standing Waves with A Posteriori Long Term Shoreline Sustainability Analysis”. en. In: *China Ocean Engineering* 35.6, pp. 802–813. DOI: [10.1007/s13344-021-0071-7](https://doi.org/10.1007/s13344-021-0071-7).
- Geuzaine, Christophe and Jean-François Remacle (2009). “Gmsh: A 3-D finite element mesh generator with built-in pre-and post-processing facilities”. In: *International journal for numerical methods in engineering* 79.11, pp. 1309–1331.
- Guo, Junke (2002). “Simple and explicit solution of wave dispersion equation”. In: *Coastal Engineering* 45.2, pp. 71–74. DOI: [https://doi.org/10.1016/S0378-3839\(02\)00039-X](https://doi.org/10.1016/S0378-3839(02)00039-X).
- Helmholtz, Professor (1868). “XLIII. On discontinuous movements of fluids”. In: *The London, Edinburgh, and Dublin Philosophical Magazine and Journal of Science* 36.244, pp. 337–346.
- Mascotto, Lorenzo, Ilaria Perugia, and Alexander Pichler (2019). “A nonconforming Trefftz virtual element method for the Helmholtz problem”. In: *Mathematical Models and Methods in Applied Sciences* 29.09, pp. 1619–1656. DOI: [10.1142/S0218202519500301](https://doi.org/10.1142/S0218202519500301).
- Munk, Walter (1949). “The solitary wave theory and its application to surf problems”. In: *Annals of the New York Academy of Sciences* 51, pp. 376–424. DOI: [10.1111/j.1749-6632.1949.tb27281.x](https://doi.org/10.1111/j.1749-6632.1949.tb27281.x).
- Perugia, Ilaria, Paola Pietra, and Alessandro Russo (2016). “A plane wave virtual element method for the Helmholtz problem”. In: *ESAIM: Mathematical Modelling and Numerical Analysis* 50.3, pp. 783–808. DOI: [10.1051/m2an/2015066](https://doi.org/10.1051/m2an/2015066).
- Talischi, Cameron, Glauco H Paulino, Anderson Pereira, and Ivan FM Menezes (2012). “PolyMesher: a general-purpose mesh generator for polygonal ele-

ments written in Matlab". In: *Structural and Multidisciplinary Optimization* 45, pp. 309–328.